Available online at www.sciencedirect.com
SCIENCE DIRECT®
Journal of Catalysis 223 (2004) 161–169
JOURNAL OF CATALYSIS
www.elsevier.com/locate/jcat

Effects of support on bifunctional methanol oxidation pathways catalyzed by polyoxometallate Keggin clusters

Haichao Liu and Enrique Iglesia *

Department of Chemical Engineering, University of California at Berkeley, Chemical Sciences Division, E.O. Lawrence Berkeley National Laboratory, Berkeley, CA 94720, USA

Received 4 November 2003; revised 26 December 2003; accepted 6 January 2004

Abstract

$H_5PV_2Mo_{10}O_{40}$ polyoxometallate Keggin clusters supported on ZrO_2, TiO_2, SiO_2, and Al_2O_3 are effective catalysts for CH_3OH oxidation reactions to form HCHO, methyl formate (MF), and dimethoxymethane (DMM). Rates and selectivities and the structure of supported clusters depend on the surface properties of the oxide supports. Raman spectroscopy showed that Keggin structures remained essentially intact on ZrO_2, TiO_2, and SiO_2 after treatment in air at 553 K, but decomposed to MoO_x and VO_x oligomers on Al_2O_3. Accessible protons per Keggin unit (KU) were measured during CH_3OH oxidation by titration with 2,6-di-*tert*-butyl pyridine. For similar KU surface densities (0.28–0.37 KU/nm^2), the number of accessible protons was larger on SiO_2 than on ZrO_2 and TiO_2 and much smaller on Al_2O_3 supports, even though residual dimethyl ether (DME) synthesis rates after titrant saturation indicated that the fractional dispersion of KU was similar on the first three supports. These effects of support on structure and on H^+ accessibility reflect varying extents of interaction between polyoxometallate clusters and supports. Rates of CH_3OH oxidative dehydrogenation per KU were higher on ZrO_2 and TiO_2 than on SiO_2 at similar KU surface densities (0.28–0.37 KU/nm^2) and dispersion, indicating that redox properties of Keggin clusters depend on the identity of the support used to disperse them. ZrO_2 and TiO_2 supports appear to enhance the reducibility of anchored polyoxometallate clusters. Rates were much lower on Al_2O_3, because structural degradation led to less reactive MoO_x and VO_x domains. CH_3OH reactions involve primary oxidation to form HCHO and subsequent secondary reactions to form DMM and MF. These reactions involve HCHO–CH_3OH acetalization steps leading to methoxymethanol (CH_3OCH_2OH) or hemiacetal intermediates, which condense with CH_3OH on acid sites to form DMM or dehydrogenate to form MF. CO_x formation rates are much lower than those of other reactions, and DME forms in parallel pathways catalyzed by acid sites. Secondary reactions leading to DMM and MF are strongly influenced by the chemical properties of support surfaces. Acidic SiO_2 surfaces favored DMM formation, while amphoteric or dehydrogenating surfaces on ZrO_2 and TiO_2 led to MF formation, as a result of the varying role of each support in directing the reactions of HCHO and CH_3OH and of the CH_3OCH_2OH intermediates toward DMM or MF, which was confirmed using physical catalyst–pure support mixtures. These support effects reflect the bifunctional pathways of CH_3OH reactions. These pathways are consistent with the effects of residence time and of the partial removal of H^+ sites by titration using 2,6-di-*tert*-butyl pyridine.
© 2004 Published by Elsevier Inc.

Keywords: Methanol oxidation; Keggin structures; Support effects; Methyl formate synthesis; Zirconia

1. Introduction

Oxidative methanol dehydrogenation reactions lead to formaldehyde (HCHO), which can react via sequential condensation or dehydrogenation reactions to form dimethoxymethane (methylal, $CH_3OCH_2OCH_3$, DMM) or methyl formate ($HCOOCH_3$, MF). Bimolecular CH_3OH dehydration occurs in parallel on acid sites to form dimethyl ether (CH_3OCH_3, DME). Selectivities are strongly influenced by acid–base and redox properties of both the redox-active components and the oxide supports [1]. Polyoxoanions with Keggin structures and charge-balancing protons or metal cations contain acid and redox sites; their number and reactivity can be controlled by varying addenda or central atoms, and the nature of the charge-balancing cations [2,3]. Thus, these materials provide suitable model structures with significant compositional and structural flexibility for catalyzing multifunctional pathways required to convert methanol to more complex and useful molecules. As a result, CH_3OH

* Corresponding author: Department of Chemical Engineering, University of California at Berkeley, Berkeley, CA 94720-1462, USA.
E-mail address: iglesia@cchem.berkeley.edu (E. Iglesia).

0021-9517/$ – see front matter © 2004 Published by Elsevier Inc.
doi:10.1016/j.jcat.2004.01.012

oxidation has been studied extensively on Keggin clusters of varying composition and catalytic functions [1,2,4–7]

We have recently reported the one-step selective synthesis of DMM via methanol oxidation at low temperatures (400–500 K) on SiO_2-supported $H_{3+n}PV_nMo_{12-n}O_{40}$ ($n = 0$–4) Keggin clusters [8]; this reaction proceeds via bifunctional pathways requiring acid and redox sites. The controlled titration or dehydroxylation of Brønsted acid sites by thermal treatment or by permanent titration with organic bases, such as pyridine, led to a selective decrease in DME formation rates, without significant changes in the rates of DMM synthesis [8,9]. The number and acid strength of the protons in Keggin clusters can also be controlled by varying the support materials and their interactions with such clusters during anchoring [2,10–12]; these supports can also introduce additional catalytic functions for reactions of the methanol reactants and of their primary HCHO products, as we show in the present study.

We report here strong effects of the support composition on the selectivity of CH_3OH–O_2 reactions catalyzed by $H_5PV_2Mo_{10}O_{40}$ clusters. This polyoxometallate composition was chosen because it led to the highest rates of CH_3OH oxidation to HCHO intermediates during DMM synthesis on silica-supported samples [8]. ZrO_2 and TiO_2 amphoteric oxides with surfaces that catalyze dehydrogenation reactions led to the selective formation of methyl formate. Unreducible oxides with weakly acidic surfaces, such as SiO_2, led predominately to dimethoxymethane. Al_2O_3-supported $H_5PV_2Mo_{10}O_{40}$ clusters led to DME with high selectivity. These supports also interacted differently with the anchored Keggin clusters and led to varying extents of deprotonation during synthesis and thermal treatment [2,10–12]. Supports influenced bifunctional methanol reactions by changing the density and type of active Keggin structures and of support active sites, in a manner that introduces significant flexibility and opportunities for designing selective catalysts for the synthesis of complex oxygenates via oxidative reactions of methanol.

2. Methods

Supported $H_5PV_2Mo_{10}O_{40}$ catalysts were prepared by incipient wetness impregnation of $ZrO(OH)_2$, SiO_2 (Cab-O-Sil, 288 m^2/g), TiO_2 (Degussa, P25), or γ-Al_2O_3 (Alcoa, HiQ31) with methanolic (Merck, 99.98%) solutions of $H_5PV_2Mo_{10}O_{40} \cdot 30H_2O$ (Japan New Metals Co.) at 298 K for 5 h. $ZrO(OH)_2$ was prepared via hydrolysis of aqueous zirconyl chloride (> 98%, Aldrich) at a pH of ~ 10 using NH_4OH (14.8 N, Fisher Scientific), subsequent filtering of precipitated powders, and drying in ambient air at 393 K overnight [13]. Surface areas were measured from N_2 adsorption uptakes at its normal boiling point (Autosorb-1; Quantachrome) using standard multipoint BET analysis methods.

Raman spectra were collected using a HoloLab 5000 spectrometer (Kaiser Optical) with a frequency-doubled Nd-YAG laser (532 nm) and a CCD camera cooled to 233 K to reduce thermal noise. Samples were pressed into self-supporting thin wafers, placed on a rotary stage within a quartz cell, and rotated at 1000 rpm to avoid local heating by the laser beam. Raman spectra were measured for fresh samples exposed to ambient air and for samples treated for 1 h in flowing 20% O_2/He (O_2, Praxair, 99.999%; He, Airgas, 99.999%; 0.67 cm^3/s) at 473–773 K.

Methanol reaction rates and selectivities were measured at 453–513 K in a packed-bed quartz microreactor using supported polyoxometallate catalysts (0.1–0.3 g; 0.18–0.25 mm) diluted with ground quartz to prevent bed temperature gradients. Samples were treated in flowing 20% O_2/He (O_2, Praxair, 99.999%; He, Airgas, 99.999%; 0.67 cm^3/s) for 1 h at 513 K before reaction rate measurements. Reactant mixtures contained CH_3OH (4 kPa; Merck, 99.98%) and O_2 (9 kPa) and N_2 (1 kPa) (Praxair, Certified O_2/N_2 mixture), with He (Airgas, 99.999%) as balance. CH_3OH was introduced by bubbling He gas through a glass saturator filled with liquid CH_3OH held at 273 K. 2,6-Di-*tert*-butyl pyridine titration measurements were carried out during methanol oxidation at 453 K in a packed-bed quartz microreactor using similarly diluted samples. Mixtures of methanol and 2,6-di-*tert*-butyl pyridine (h-pyridine; Aldrich, 97%) with a 1110:1 molar ratio were introduced by continuous liquid injection using a microsyringe pump (Cole-Parmer 74900). All transfer lines between the point of liquid introduction and the gas chromatograph were kept above 393 K to avoid condensation. Reactants and products were analyzed by on-line chromatography (Hewlett–Packard 6890GC) using a methyl-silicone capillary column (HP-1; 30 m × 0.25 mm, 0.25-μm film thickness) and a Porapak Q packed column (80–100 mesh, 1.82 m × 3.18 mm) connected to flame ionization and thermal conductivity detectors, respectively. Selectivities are reported on a carbon basis as the percentage of the converted CH_3OH appearing as a given product, and rates are reported as the number of CH_3OH molecules converted into a given product per Keggin unit per hour. Experiments using empty reactors did not lead to detectable CH_3OH conversions under any of the conditions in this study.

3. Results and discussion

Table 1 lists methanol conversion rates and selectivities on $H_5PV_2Mo_{10}O_{40}$ supported on ZrO_2, TiO_2, and Al_2O_3 at 493 K, and for comparison, also on SiO_2 supports from our previous study [8]. These samples contain similar densities of Keggin units (0.28–0.37 KU/nm^2). Kinetic comparisons are made at similar CH_3OH conversion levels (30–40%), because relative contributions from primary and secondary reactions depend on residence time and conversion, as discussed below. Reaction rates reported in Table 1 are normalized per Keggin unit and reported on a DME-free basis

Table 1
Methanol oxidation rates, selectivities, and number of accessible Brønsted acid sites on $H_5PV_2Mo_{10}O_{40}$ supported on ZrO_2, TiO_2, SiO_2, and Al_2O_3 (treated at 553 K) and on bulk $H_5PV_2Mo_{10}O_{40}$ and pure supports (493 K, 4% CH_3OH, 9% O_2, 1% N_2, He balance, 30–40% CH_3OH conversion)

Catalyst	Surface density	Brønsted acid	Rate (DME-free)	ODH rate	Selectivity (% carbon)				
	(KU/nm^2)	sites (H^+/KU)[b]	(molecules/(KU h))	(molecules/(KU h))	DME	HCHO	MF	DMM	CO_x
$H_5PV_2Mo_{10}O_{40}/ZrO_2$	0.31	0.92	213.7	127.8	16.1	21.2	52.4	8.3	2.0
$H_5PV_2Mo_{10}O_{40}/SiO_2$	0.28	1.24	190.9	79.7	36.5	8.1	2.7	51.2	0
$H_5PV_2Mo_{10}O_{40}/TiO_2$	0.37	0.86	195.2	146.0	9.5	53.2	30.2	7.1	0
$H_5PV_2Mo_{10}O_{40}/Al_2O_3$	0.35	0.41	51.2	41.3	71.1	19.2	5.1	4.6	0
Bulk $H_5PV_2Mo_{10}O_{40}$	–	0.02	5.5	2.6	48.1	8.7	0.4	40.2	2.6
ZrO_2	–	–	Trace	–	–	–	–	–	–
SiO_2	–	–	Trace	–	–	–	–	–	–
TiO_2	–	–	Trace	–	–	–	–	–	–
Al_2O_3	–	–	26.0[a]	–	100	0	0	0	0

[a] CH_3OH conversion rate: mmol/g Al_2O_3 per hour at 34% CH_3OH conversion.
[b] From 2, b di-tert-butyl pyridine uptakes during catalysis.

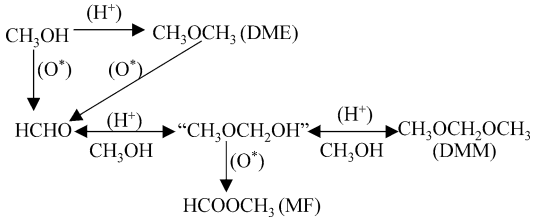

Scheme 1. Proposed primary and secondary CH_3OH reaction pathways.

(conversion to all products except DME). Pure Al_2O_3 supports formed only DME, while other pure supports did not form products at detectable rates. CH_3OH conversion rates were slightly higher when $H_5PV_2Mo_{10}O_{40}$ clusters were supported on ZrO_2 and TiO_2 than when supported on SiO_2, and they were much lower when supported on Al_2O_3 than on all other supports (Table 1).

CH_3OH oxidation occurs via rate-determining C–H bond activation steps in methoxy groups to form HCHO via redox cycles catalyzed by Keggin clusters [1]. HCHO can then react in subsequent reactions with methanol to form hemiacetal or methoxymethanol intermediates (CH_3OCH_2OH) [14–16], which can undergo condensation reactions with CH_3OH to form DMM or hydrogen abstraction to form MF (Scheme 1). Reactions listed along the horizontal direction in Scheme 1 require Brønsted acid sites, while those represented by vertical arrows involve reactive forms of oxygen (O^*) from either Keggin clusters or active supports.

In Scheme 1, the irreversible nature of the oxidative conversion of CH_3OH to HCHO implies that each HCHO, DMM, and MF product requires one oxidative CH_3OH dehydrogenation event; thus, the rates of the latter step are given by the sum of the molar rates of formation of these products. These oxidative dehydrogenation (ODH) rates are 1.5–1.8 times greater on ZrO_2 and TiO_2 than on SiO_2 (Table 1), apparently as a result of the higher redox reactivity and ability to undergo catalytic redox cycles for Keggin clusters supported on ZrO_2 and TiO_2 than on SiO_2, as in previously reported trends for MoO_x and VO_x domains on these supports [17,18]. The more reducible nature of TiO_2 and ZrO_2 surfaces typically leads to more reducible oxide domains than more refractory and acidic SiO_2 and Al_2O_3 surfaces [13,17,18]. $H_5PV_2Mo_{10}O_{40}$ precursors supported on Al_2O_3 were less reactive for oxidative dehydrogenation reactions than on other supports also because of structural degradation of Keggin clusters on Al_2O_3 to form MoO_x and VO_x domains (as discussed below), which undergo redox cycles more slowly than intact Keggin clusters, as previously shown also on SiO_2 surfaces [8].

The identity of the support also influences CH_3OH reaction selectivities on $H_5PV_2Mo_{10}O_{40}$ clusters at all CH_3OH conversions; these selectivity comparisons are made at 30–40% CH_3OH conversion, but the trends remain at all conversion levels. On SiO_2, DMM is the main product (51.2%) along with DME (36.5%), while MF is formed with very low selectivity (2.7%) [8]. In marked contrast, MF became the predominant product (52.4%) and DMM selectivities were very low (8.3%) when ZrO_2 was used as the support instead of SiO_2 (Table 1). DME selectivities were much lower on $H_5PV_2Mo_{10}O_{40}/ZrO_2$ than on SiO_2-supported samples (16.1 vs 36.5%). On TiO_2 supports, $H_5PV_2Mo_{10}O_{40}$ clusters formed predominantly HCHO (53.2%); the MF selectivity was 30.2%, with very low DME and DMM selectivities (9.5 and 7.1%, respectively). This appears to reflect the lower reactivity of TiO_2 supports for secondary reactions of HCHO–CH_3OH mixtures to form MF compared with ZrO_2 surfaces, which preserves a larger fraction of the primary HCHO products in the reacting mixture. CH_3OH dehydration to DME became the predominant reaction ($\sim$ 71% selectivity) on $H_5PV_2Mo_{10}O_{40}/Al_2O_3$ (Table 1), as expected from the reactivity of Lewis acid sites on Al_2O_3 supports in bimolecular CH_3OH dehydration reactions. These support effects are consistent with the observed changes in acidity and with the observed structural evolution of $H_5PV_2Mo_{10}O_{40}$ clusters on these supports, which were probed by organic base titration (i.e., 2,6-di-*tert*-butyl pyridine) and Raman spectroscopy, respectively, as we discuss immediately below.

Fig. 1 shows the Raman spectra for $H_5PV_2Mo_{10}O_{40}$ supported on SiO_2, ZrO_2, TiO_2, and Al_2O_3 (0.28–0.40 KU/nm^2) after exposure to ambient air at 298 K (Fig. 1a) and after treatment in flowing dry air at 553 K within the Raman

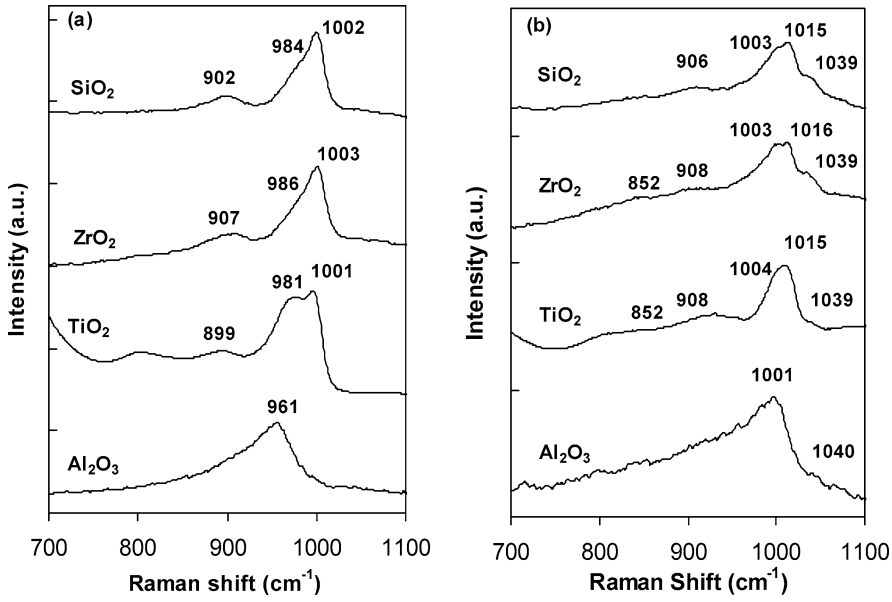

Fig. 1. Raman spectra for $H_5PV_2Mo_{10}O_{40}$ supported on SiO_2, ZrO_2, TiO_2, and Al_2O_3 with surface densities of 0.28–0.37 KU/nm^2 at ambient conditions (a) and after treatment in flowing dry air at 553 K for 1 h (b).

cell (Fig. 1b). $H_5PV_2Mo_{10}O_{40}/ZrO_2$ samples exposed to ambient moisture showed Raman bands at 1003 (s), 986 (sh), and $\sim$ 907 (w) cm^{-1} in the range 700–1100 cm^{-1} (Fig. 1a). The bands at 1003 and 986 cm^{-1} are assigned to terminal Mo=O stretching vibrations, and the band around 907 cm^{-1} to bridging Mo–O–Mo (or Mo–O–P) stretching modes in intact Keggin structures [19]. Terminal Mo=O stretching bands at 1002 and 984 cm^{-1} shifted to higher frequencies 1016 and 1003 cm^{-1}, respectively, after treatment in 20% O_2/He at 553 K, while the band at 907 cm^{-1} was essentially unchanged by this treatment (Fig. 1b). The observed shift to higher frequencies on thermal treatment and the concurrent water desorption reflect changes in Mo coordination and in bond orders for terminal Mo=O bonds, caused by desorption of water loosely coordinated within the secondary crystal structure of the polyoxometallate clusters [20].

Two new weak bands appeared at 1039 and 852 cm^{-1} after treatment at 553 K; the 1039 cm^{-1} band was tentatively assigned to vanadyl species formed by removal of some of the V atoms in $H_5PV_2Mo_{10}O_{40}$ clusters during thermal treatment [19]. The weak broad band at 852 cm^{-1} was assigned to amorphous β-MoO_3 [5,10], indicating some limited structural degradation of supported Keggin clusters during treatment at 553 K. The strengthening of the 1003 cm^{-1} band relative to that at 1015 cm^{-1} after treatment at 553 K (Fig. 1b) appears to reflect the loss of some protons via dehydroxylation, with the consequent formation of condensed Keggin structures. Exposure to ambient moisture, however, led to full recovery of the initial spectra for $H_5PV_2Mo_{10}O_{40}$ clusters, indicating that dehydroxylation is reversible and does not lead to any significant destruction of the Keggin structures; this recovery is also expected to occur as water forms during CH_3OH oxidation catalysis. After CH_3OH oxidation reactions, catalysts showed very weak Raman bands, as a result of absorption of incident and scattered photons by color centers, which form as reactive intermediates during catalytic redox cycles. Treatment in dry air at 553 K and exposure to ambient moisture, however, led to the full recovery of the spectra for the respective fresh samples, indicating that supported Keggin structures do not restructure irreversibly during CH_3OH oxidation catalysis.

These Raman features and their evolution during thermal treatment are similar to those detected for $H_5PV_2Mo_{10}O_{40}$ clusters on TiO_2 (Fig. 1a and b) and to those reported previously for $H_5PV_2Mo_{10}O_{40}$ clusters on SiO_2 [8], except that no β-MoO_3 bands at $\sim$ 852 cm^{-1} appeared on SiO_2 supports (Fig. 1b) after treatment at 553 K. $H_5PV_2Mo_{10}O_{40}$ clusters on Al_2O_3 decomposed to two-dimensional MoO_x oligomers, as shown by the typical Raman band at 962 cm^{-1} for terminal Mo=O stretching vibrations in MoO_x species, which shifted to 1001 cm^{-1} (Fig. 1) upon dehydration at 553 K [20,21]. These differences reflect the varying degree of interaction of Keggin polyoxometallate clusters with each support.

The number of accessible protons in $H_5PV_2Mo_{10}O_{40}$ polyoxometallate structures was measured by titration with sterically hindered pyridine (2,6-di-*tert*-butyl pyridine) during catalytic CH_3OH reactions. 2,6-Di-*tert*-butyl pyridine titrant is protonated by Brønsted acids, but steric constraints prevent its coordination to Lewis acid sites via nitrogen lone electron pairs [22]. Saturation 2,6-di-*tert*-butyl pyridine uptakes reflect the number of accessible protons. The number of 2,6-di-*tert*-butyl pyridine molecules adsorbed during CH_3OH–O_2 reactions at 453 K on $H_5PV_2Mo_{10}O_{40}/ZrO_2$ (0.31 KU/nm^2) increased with time during titration and reached saturation values of 0.92 per KU (Fig. 2). Saturation titrant uptakes are listed in Table 1 for $H_5PV_2Mo_{10}O_{40}$ supported on ZrO_2, TiO_2, and SiO_2; these saturation up-

takes (0.86–1.24 per KU) are smaller than expected from the $H_5PV_2Mo_{10}O_{40}$ stoichiometry (5 per KU), apparently because dehydroxylation occurs among clusters and with support OH groups and because the dispersion of Keggin clusters on supports is incomplete. Titrant/KU values on SiO_2 are greater than on ZrO_2 and TiO_2, consistent with the strong interaction reported between Keggin structures and ZrO_2 and TiO_2 surfaces [10–12]; these lower proton densities also led to lower DME selectivities on ZrO_2 and TiO_2 than on SiO_2 during CH_3OH reactions (Table 1). $H_5PV_2Mo_{10}O_{40}$ clusters decomposed on Al_2O_3, leading to low densities of Brønsted acid sites on Al_2O_3 (0.4 H^+/KU) (Table 1); the high DME selectivities observed reflect Lewis acid-catalyzed dehydration pathways on Al_2O_3 surfaces.

Titration of Brønsted acid sites by 2,6-di-*tert*-butyl pyridine during methanol reactions decreased the rates for both bifunctional DMM and monofunctional DME synthesis steps on $H_5PV_2Mo_{10}O_{40}/ZrO_2$; both rates reached nonzero constant values even after saturated 2,6-di-*tert*-butyl pyridine adsorption (0.92 per KU) (Fig. 2). These residual rates reflect the apparent ability of CH_3OH reactants to access protons within secondary structures that larger and less polar 2,6-di-*tert*-butyl pyridine molecules cannot readily reach. DME formation rates were influenced more strongly than DMM formation rates by titration with 2,6-di-*tert*-butyl pyridine on $H_5PV_2Mo_{10}O_{40}/ZrO_2$, as previously shown on $H_5PV_2Mo_{10}O_{40}/SiO_2$ [9]. This suggests that acid-catalyzed steps required for bifunctional DMM formation are near thermodynamic equilibrium in the proposed pathways for DMM and DME synthesis (Scheme 1). Bimolecular CH_3OH dehydration to DME remains far from equilibrium and it is therefore much more sensitive to the remaining number of Brønsted acid sites. The monofunctional and nonequilibrated nature of DME synthesis pathways and the different accessibility of methanol and hindered pyridine molecules provide an indirect method for measuring the degree of dispersion of polyoxometallate clusters on various supports. The fraction of the DME synthesis rates before titrant addition that remains after saturated adsorption by 2,6-di-*tert*-butyl pyridine provides a measure of inaccessible protons. These ratios are 0.085, 0.081, and 0.090 on ZrO_2, TiO_2, and SiO_2, respectively, suggesting that polyoxometallate $H_5PV_2Mo_{10}O_{40}$ clusters are dispersed to similar extents on these three supports. On Al_2O_3, DME formation rates were essentially independent of 2,6 di-*tert*-butyl pyridine adsorption, because DME forms preferentially on Lewis acid sites, which do not interact with 2,6 di-*tert*-butyl pyridine titrants. MF and HCHO formation rates also decreased to constant values as Brønsted acid sites were titrated (Fig. 2). The observed decrease in CH_3OH dehydrogenation rates indicates that replacement of H^+ by electron-rich alkylpyridinium cations decreases the reducibility of polyoxometallate Keggin clusters. This is consistent with the expected electron transfer to Mo and V cations, which strengthens Mo–O and V–O bonds and decreases the extent to which electron density can be delocalized within oxide clusters during reduction processes required for catalytic cycles.

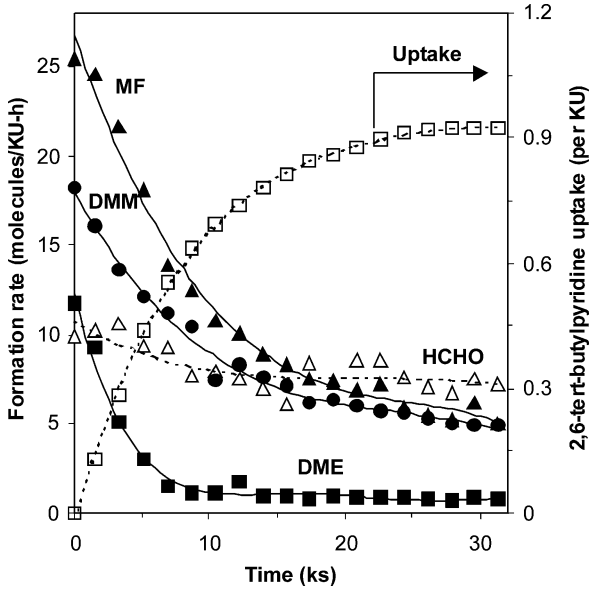

Fig. 2. Adsorption uptakes and rates for DME, HCHO, DMM, and MF formation as a function of time-on-stream during 2,6-di-*tert*-butyl-pyridine addition to $H_5PV_2Mo_{10}O_{40}/ZrO_2$ (0.31 KU/nm^2, 453 K, 4 kPa CH_3OH, 9 kPa O_2, CH_3OH/2,6-di-*tert*-butyl-pyridine (mol) = 1110).

The role of supports on secondary reactions of the HCHO molecules formed in primary methanol oxidation reactions was examined by mixing supported $H_5PV_2Mo_{10}O_{40}$ catalysts with additional amounts of pure supports. As shown in Table 2, adding ZrO_2 to $H_5PV_2Mo_{10}O_{40}/SiO_2$ (3:1 mass ratio) at 493 K increased MF selectivity from 2.7 to 42.3%, while DMM selectivity decreased from 51.2 to 8.9%. The addition of TiO_2 to $H_5PV_2Mo_{10}O_{40}/SiO_2$ (3:1 mass ra-

Table 2
Methanol oxidation rates and selectivities on physical mixtures of $H_5PV_2Mo_{10}O_{40}/SiO_2 + ZrO_2$, $H_5PV_2Mo_{10}O_{40}/ZrO_2 + SiO_2$, and $H_5PV_2Mo_{10}O_{40}/SiO_2 + TiO_2$ at a mass ratio of 1/3, and for comparison on $H_5PV_2Mo_{10}O_{40}/SiO_2$ (0.28 KU/nm^2) and $H_5PV_2Mo_{10}O_{40}/ZrO_2$ (0.31 KU/nm^2) treated at 553 K (493 K, 4% CH_3OH, 9% O_2, 1% N_2, 30–40% CH_3OH conversion)

Catalyst (mass ratio)	Conversion rate (DME-free)	ODH rate	Selectivity (% carbon)				
	(molecules/(KU h))	(molecules/(KU h))	DME	HCHO	MF	DMM	CO_x
$H_5PV_2Mo_{10}O_{40}/SiO_2 + ZrO_2$ (1/3)	174.3	83.9	35.4	7.0	42.3	8.9	6.4
$H_5PV_2Mo_{10}O_{40}/ZrO_2 + SiO_2$ (1/3)	211.3	122.9	15.3	19.1	46.2	18.1	1.3
$H_5PV_2Mo_{10}O_{40}/SiO_2 + TiO_2$ (1/3)	164.7	83.4	33.3	14.5	29.2	17.8	5.2
$H_5PV_2Mo_{10}O_{40}/SiO_2$	190.9	79.7	36.5	8.1	2.7	51.2	0
$H_5PV_2Mo_{10}O_{40}/ZrO_2$	213.7	127.8	16.1	21.2	52.4	8.3	2.0

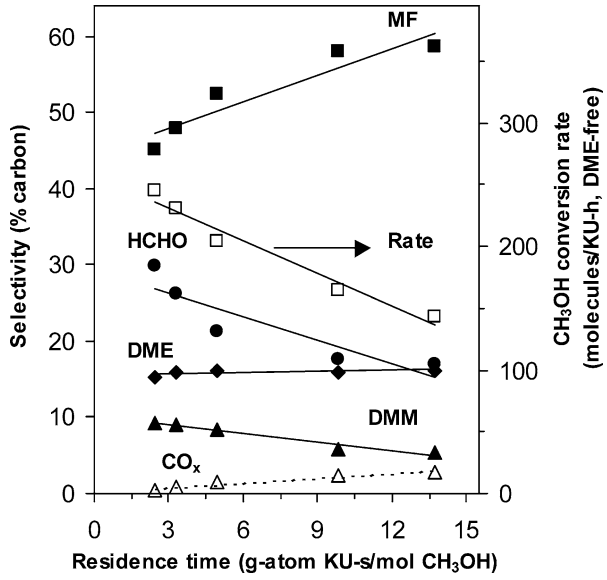

Fig. 3. CH_3OH conversion rates (on a DME-free basis) and selectivities as a function of residence time at 493 K on $H_5PV_2Mo_{10}O_{40}/ZrO_2$ (0.31 KU/nm^2, 4 kPa CH_3OH, 9 kPa O_2, 1 kPa N_2, CH_3OH conversion 18.6–65.8%).

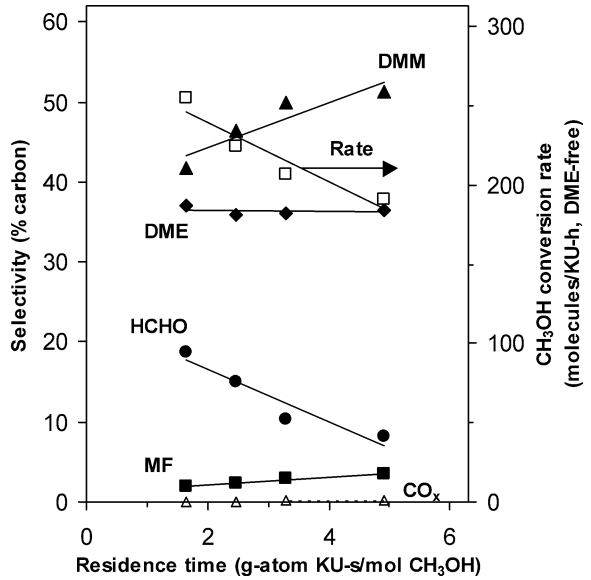

Fig. 4. CH_3OH conversion rates (on a DME-free basis) and selectivities as a function of residence time at 493 K on $H_5PV_2Mo_{10}O_{40}/SiO_2$ (0.28 KU/nm^2, 4 kPa CH_3OH, 9 kPa O_2, 1 kPa N_2, CH_3OH conversion 21.3–47.6%).

tio) led to MF and DMM selectivities of 29.2 and 17.8% (vs 2.7 and 51.2% without TiO_2), respectively. Thus, ZrO_2 and TiO_2 support surfaces can convert HCHO–CH_3OH mixtures to MF, or possibly intercept reactive intermediates and convert them to MF before they condense with CH_3OH to form DMM on acidic sites on SiO_2 or Keggin clusters. The stronger effects of added ZrO_2 relative to TiO_2 are consistent with the higher MF selectivities obtained when ZrO_2 is used directly to support polyoxometallate clusters (Table 1). In contrast, when pure SiO_2 (3:1 mass ratio) was added to $H_5PV_2Mo_{10}O_{40}/ZrO_2$, DMM selectivities increased from 8.3 to 18.1%, indicating that SiO_2 surfaces direct HCHO–CH_3OH reactions toward DMM before dehydrogenation events leading to MF can occur. None of the experiments in which pure supports were mixed with supported $H_5PV_2Mo_{10}O_{40}$ catalysts led to detectable increases in the rates for oxidative dehydrogenation (ODH) of CH_3OH to HCHO (Table 2). The minor changes in CH_3OH conversion rates observed merely reflect the different reaction stoichiometries required for DMM and MF formation in secondary reactions of HCHO with CH_3OH (Scheme 1), the relative rates of which were influenced by the presence of the pure supports in these physical mixtures.

Fig. 3 shows the effects of reactant residence time, changed by varying the space velocity, on methanol conversion rates and selectivities at 493 K on $H_5PV_2Mo_{10}O_{40}/ZrO_2$ (0.31 KU/nm^2). Rates decreased with increasing residence time and methanol conversion, as a result of reactant depletion and of weak kinetic inhibition effects by the water products formed during reaction. MF selectivities increased with increasing residence time and methanol conversion, consistent with the secondary nature of the reactions leading to its synthesis, while HCHO and DMM selectivities concurrently decreased. This decrease in DMM selectivity appears to reflect the reversible nature of condensation reactions, which approach equilibrium as conversion increases with increasing residence time. CO_x selectivities remained very low (0–2.5%) at all conversion levels, but increased with increasing residence time, suggesting that CO_x forms preferentially via secondary reactions of HCHO, MF, and DMM products. DME selectivities were essentially unchanged by residence time, consistent with the formation of DME in parallel reactions and with its lower reactivity in HCHO formation reactions compared with CH_3OH reactants [8]. Fig. 4 shows similar residence time effects on $H_5PV_2Mo_{10}O_{40}/SiO_2$ (0.28 KU/nm^2). On this catalyst, DMM selectivities increased monotonically with residence time, apparently because SiO_2 does not scavenge DMM or its methoxymethanol-type (CH_3OCH_2OH) intermediates via dehydrogenation reactions that form MF on ZrO_2 or TiO_2 supports. The trends with residence time for CH_3OH conversion rates and for selectivities to other products (HCHO, MF, CO_x, and DME) are similar on $H_5PV_2Mo_{10}O_{40}/SiO_2$ and $H_5PV_2Mo_{10}O_{40}/ZrO_2$.

DMM conversion to MF was confirmed by reactions of DMM–O_2 and CH_3OH–DMM–O_2 reactant mixtures on $H_5PV_2Mo_{10}O_{40}/ZrO_2$. Table 3 shows that addition of 2 kPa DMM to CH_3OH (4 kPa)/O_2 (9 kPa) reactants led to an increase in MF formation rates by ~ 1.7 at 493 K, indicating that reversible reactions of DMM during methanol oxidation indeed lead to MF formation, possibly via scavenging of methoxymethanol-type or hemiacetal intermediates (Scheme 1). DMM reactions also formed HCHO, CH_3OH, and DME, as expected from the reversible nature of condensation reaction during CH_3OH reactions on surfaces containing Brønsted acid sites.

Table 3
MF formation rates and product selectivities in oxidation reactions of DMM (2 kPa), a DMM (2 kPa) and CH_3OH (4 kPa) mixture, and, for comparison, CH_3OH (4 kPa) on $H_5PV_2Mo_{10}O_{40}/ZrO_2$ (0.31 KU/nm^2, 493 K, 9% O_2, 1% N_2, 30–40% CH_3OH or DMM conversion)

Reactant	MF formation rate	Selectivity (%)					
	(MF molecules/(KU h))	CH_3OH	DME	HCHO	MF	DMM	CO_x
CH_3OH	66.8	–	16.1	21.2	52.4	8.3	2.0
DMM	89.2	28.1	14.3	17.6	39.7	–	0.2
DMM + CH_3OH	112.4	–	–	–	–	–	–

These observed effects of residence time and support on selectivities are consistent with the reaction pathways shown in Scheme 1. These pathways include primary reactions of CH_3OH to form DME and HCHO and secondary reactions of HCHO to form DMM and MF via methoxymethanol (CH_3OCH_3OH) or hemiacetal adsorbed intermediates. HCHO acetalization with nucleophilic methoxides (CH_3O^-) forms CH_3OCH_2OH-type intermediates [14–16], which either condense with another CH_3OH molecule on acid sites to form DMM in equilibrium-constrained reactions or dehydrogenate to form MF in reactions favored by thermodynamics when O_2 is used to form H_2O.

A theoretical study has suggested that CH_3OCH_2OH dehydrogenation on V_2O_5 is the preferred MF synthesis path compared with the other two possible pathways: HCHO dimerization (Tischenko reaction) and CH_3OH reaction with adsorbed formate ($HCOO^-$) intermediates [23]. CH_3OCH_2OH was not detected during CH_3OH reactions on $H_5PV_2Mo_{10}O_{40}$, because of its very reactive nature and its unfavorable thermodynamics. The rapid reactions of HCHO and CH_3OCH_2OH intermediates with CH_3OH make DMM and MF appear to behave as primary products, giving nonzero extrapolated selectivities at zero residence time (Figs. 3 and 4). The low measured CO_x selectivities ($< 2.5\%$) allow us to exclude CO_x formation steps from our kinetic analysis of these reaction pathways. Previous DME oxidation kinetic measurements [8] suggest that secondary reactions of DME formed in CH_3OH reactions can also form HCHO, which subsequently converts to DMM and MF (Scheme 1). These reaction pathways (Scheme 1) require bifunctional pathways involving both redox and acid sites. Redox sites with active lattice oxygen atoms catalyze initial oxidative dehydrogenation reactions of CH_3OH or DME to form HCHO and subsequent (oxidative or non-oxidative) dehydrogenation of CH_3OCH_2OH intermediates to form MF, while acid sites (H^+) are involved in the formation of CH_3OCH_2OH intermediates and in their conversion to DMM, as well as in CH_3OH dehydration to form DME.

The effects of reaction temperature on CH_3OH conversion rates and selectivities are shown in Fig. 5. Rates increased from 58.6 to 373.7 molecules/(KU h) on $H_5PV_2Mo_{10}O_{40}/ZrO_2$ (0.31 KU/nm^2) as the temperature increased from 453 to 513 K at similar CH_3OH conversions (30–40%; kept constant by varying residence time). HCHO and MF selectivities increased from 13.5 to 27.9% and from 42.5 to 52.4%, respectively, as temperature increased, while

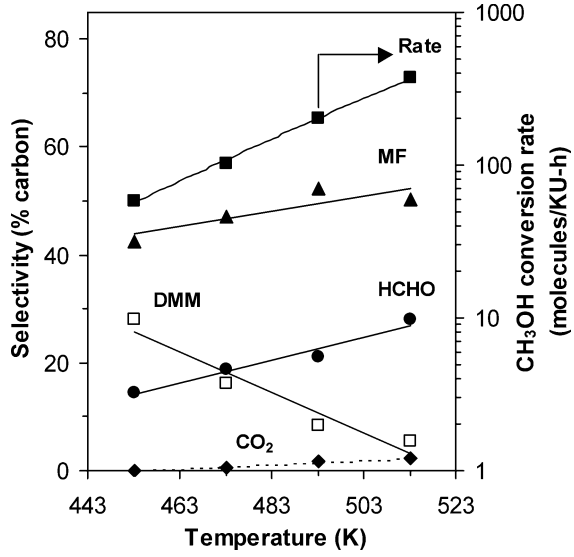

Fig. 5. CH_3OH conversion rates (on a DME-free basis) and selectivities as a function of reaction temperature on $H_5PV_2Mo_{10}O_{40}/ZrO_2$ (0.31 KU/nm^2, 4 kPa CH_3OH, 9 kPa O_2, 1 kPa N_2, CH_3OH conversion 30–40%).

DMM selectivities decreased from 28.4 to 5.6%. These temperature effects indicate that rates of redox reactions (forming HCHO and MF) are more sensitive to temperature than net rates of DMM synthesis, possibly as a result of thermodynamic constraints for the latter reaction. Oxidative dehydrogenation of CH_3OH to HCHO is thermodynamically favorable ($\Delta G^0 = -186.4$ to -190.6 kJ/mol at 453 and 513 K) [1,24] and far from equilibrium. DMM and MF form via subsequent reactions of HCHO with CH_3OH via CH_3OCH_2OH intermediates (Scheme 1). The value of ΔG^0 for DMM formation,

$$2CH_3OH + HCHO \leftrightarrow CH_3OCH_2OCH_3 + H_2O,$$

decreased from -15.0 to -7.7 kJ/mol, and its equilibrium rate constant decreased sharply from 53.7 to 6.5 as temperature increased from 453 to 513 K; ΔG^0 values for DMM are not available and were estimated using density functional theory (B3LYP/6-31G*), while ΔG^0 values for all other compounds were obtained from the literature [24]. In contrast, MF formation,

$$CH_3OH + HCHO + \tfrac{1}{2}O_2 \leftrightarrow HCOOCH_3 + H_2O,$$

is far from equilibrium ($\Delta G^0 = -242.7$ to -238.9 kJ/mol at 453–513 K). Higher temperatures thus favor the C–H bond activation in CH_3OH to HCHO, and the reactions of

Table 4
Methanol conversion rates (DME-free basis), selectivities, and number of accessible Brønsted acid sites as a function of $H_5PV_2Mo_{10}O_{40}$ surface density on ZrO_2 (493 K, 4% CH_3OH, 9% O_2, 1% N_2, 30–40% CH_3OH conversion)

Surface density (KU/nm^2)	Brønsted acid sites (H^+/KU)	Conversion rate (DME-free) (molecules/(KU h))	ODH rate (molecules/(KU h))	Selectivity (% carbon)				
				DME	HCHO	MF	DMM	CO_x
0	–	Trace	Trace	–	–	–	–	–
0.08	0.68	97.8	52.0	9.8	7.6	77.6	2.8	2.3
0.15	0.84	145.6	76.8	10.4	8.9	72.8	5.9	2.1
0.31	0.93	213.7	127.8	16.1	21.2	52.4	8.3	2.0

DMM and CH_3OCH_2OH intermediates to HCHO, CH_3OH, and MF instead of DMM. This leads to the lower DMM selectivities and higher HCHO and MF selectivities observed as temperature increases. Selectivities to by-products DME ($\sim 15\%$) and CO_x ($< 2.2\%$) were only weakly affected by reaction temperature (Fig. 5).

A parallel study addressed the effects of $H_5PV_2Mo_{10}O_{40}$ surface density on catalytic properties. Table 4 shows that methanol conversion and ODH rates (per KU) increased by factors of 2.2 and 2.5, respectively, as the surface density of Keggin units increased from 0.08 to 0.31 KU/nm^2. In this surface density range, the fractions of initial DME synthesis rates remaining after 2.6 di-*tert*-butyl pyridine saturation are similar for all samples (0.081–0.087), suggesting that the extent of exposure to reactants is also independent of surface density. Thus, the higher reaction rates (per KU) observed with increasing surface density reflect a higher reactivity of polyoxometallate clusters as the domain size of two-dimensional agglomerates of polyoxometallate clusters increased with increasing surface density. The larger domains prevalent at higher surface densities appear to undergo faster redox cycles required for methanol oxidation than the isolated or small domains at lower surface density, as also found for simple oxide domains of MoO_x and VO_x [9,21,25]. MF selectivities decreased from 77.6 to 52.4% as the polyoxometallate surface densities increased, apparently because the ratio of exposed ZrO_2 to polyoxometallate surfaces decreased, leading to smaller contributions from ZrO_2-catalyzed MF synthesis pathways. The number of accessible Brønsted acid sites (H^+), estimated by the saturated 2,6-*tert*-butyl pyridine uptakes, increased slightly from 0.68 to 0.93 H^+/KU as the surface density increased from 0.08 to 0.31 KU/nm^2. This led to the observed concurrent increase in DME and DMM selectivities (Table 4), consistent with the acid sites required for their respective formation.

4. Conclusions

$H_5PV_2Mo_{10}O_{40}$ polyoxometallate Keggin clusters supported on ZrO_2, TiO_2, SiO_2, and Al_2O_3 catalyze CH_3OH oxidation reactions to form HCHO, DMM, and MF. These Keggin structures remain essentially intact on ZrO_2, TiO_2, and SiO_2 after treatment in air at 553 K, but decompose to MoO_x and VO_x oligomers on Al_2O_3. For similar KU surface densities (0.28–0.37 KU/nm^2), the number of accessible protons is larger on SiO_2 than on ZrO_2 and TiO_2 and much smaller on Al_2O_3 supports. These effects of support on structure and H^+ accessibility reflect varying extents of interaction between polyoxometallate clusters and supports. Rates of CH_3OH oxidative dehydrogenation per KU are higher on ZrO_2 and TiO_2 than on SiO_2 at similar KU surface densities (0.28–0.37 KU/nm^2) and dispersions, indicating that redox properties and catalytic reactivity of Keggin clusters depend on their atomic attachment to specific support surfaces. Rates are much lower on Al_2O_3, because structural degradation leads to less reactive MoO_x and VO_x domains. CH_3OH undergoes primary oxidation to form HCHO and subsequent secondary reactions to form DMM and MF via methoxymethanol (CH_3OCH_2OH) intermediates in steps requiring the bifunctional acid and redox sites; DME forms in parallel pathways catalyzed by acid sites. The identity of the support strongly influences the secondary reaction pathways leading to DMM and MF. Amphoteric or dehydrogenating surfaces on ZrO_2 and TiO_2 lead to MF formation, while DMM formation is favored by the presence of acidic SiO_2 surfaces. The lower DME selectivities on ZrO_2 and TiO_2 than on SiO_2 are consistent with fewer H^+ sites per KU on ZrO_2 and TiO_2 than on SiO_2, as measured by titration with 2,6 di-*tert*-butyl pyridine during CH_3OH reactions. Al_2O_3 supports lead to DME as the dominant product because of the available Lewis acid-catalyzed dehydration pathways on Al_2O_3 surfaces and the low reactivity of MoO_x and VO_x domains.

Acknowledgments

This work was supported in part by BP as part of the Methane Conversion Cooperative Research Program at the University of California at Berkeley and by the Director, Office of Basic Energy Sciences, Chemical Sciences Division, of the U.S. Department of Energy under Contract DE-AC03-76SF00098. The authors thank Ms. Patricia Cheung for the ΔG^0 estimates for DMM. The authors also acknowledge helpful technical discussions with Dr. Theo Fleisch of BP.

References

[1] J.M. Tatibouet, Appl. Catal. 148 (1997) 213.
[2] T. Okuhara, N. Mizuno, M. Misono, Adv. Catal. 41 (1994) 113.
[3] M. Misono, J. Chem. Soc. Chem. Commun. (2001) 1141.

[4] C.M. Sorensen, R.S. Weber, J. Catal. 142 (1993) 1.
[5] C. Rocchiccioli-Deltcheff, A. Aouissi, S. Launay, M. Fournier, J. Mol. Catal. 114 (1996) 331.
[6] C. Rocchiccioli-Deltcheff, A. Aouissi, M.M. Bettahar, S. Launay, M. Fournier, J. Catal. 164 (1996) 16.
[7] K. Buckman, J.M. Tatibouet, M. Che, E.M. Serwicka, J. Haber, J. Catal. 139 (1993) 455.
[8] H. Liu, E. Iglesia, J. Phys. Chem. B 107 (2003) 10840.
[9] H. Liu, N. Bayat, E. Iglesia, Angew. Chem. Int. Ed. 42 (2003) 5072.
[10] S. Damyanova, L.M. Gomez Sainerro, J.L.G. Fierro, Chem. Mater. 12 (2000) 501.
[11] S. Damyanova, J.L.G. Fierro, Chem. Mater. 10 (1998) 871.
[12] P.G. Vazquez, M.N. Blanco, C.V. Caceres, Catal. Lett. 60 (1999) 205.
[13] H. Liu, P. Cheung, E. Iglesia, J. Catal. 217 (2003) 222.
[14] C. Louis, J.M. Tatibouet, M. Che, J. Catal. 109 (1988) 354.
[15] I.E. Wachs, R.J. Madix, Surf. Sci. 76 (1978) 531.
[16] J.M. Tatibouet, H. Lauron-Pernot, J. Mol. Catal. A 171 (2001) 205.
[17] A.N. Desikan, W. Zhang, S.T. Oyama, J. Catal. 157 (1995) 740.
[18] G. Deo, I.E. Wachs, J. Catal. 146 (1994) 323.
[19] G. Mestl, T. Ilkenhans, D. Spielbauer, M. Dieterle, O. Timpe, J. Krohnert, F. Jentoft, H. Knozinger, R. Schlogl, Appl. Catal. A 210 (2001) 13.
[20] G. Mestl, T.K.K. Srinivasan, Catal. Rev. Sci. Eng. 38 (1998) 451.
[21] K. Chen, S. Xie, A.T. Bell, E. Iglesia, J. Catal. 198 (2001) 232.
[22] J.G. Santiesteban, J.C. Vartuli, S. Han, R.D. Bastian, C.D. Chang, J. Catal. 168 (1997) 431.
[23] J. Sabeth, A. Juan, L. Gambaro, H. Thomas, J. Mol. Catal. A 118 (1997) 283.
[24] D.R. Stull, F. Edgar, J. Westrum, G.C. Sinke, in: The Chemical Thermodynamics of Organic Compounds, Robert E. Krieger, Malabar, FL, 1987.
[25] H. Liu, P. Cheung, E. Iglesia, Phys. Chem. Chem. Phys. 5 (2003) 3795.